BATTERIES

Reversible epitaxial electrodeposition of metals in battery anodes

Jingxu Zheng[1]*, Qing Zhao[2]*, Tian Tang[1], Jiefu Yin[2], Calvin D. Quilty[3], Genesis D. Renderos[3], Xiaotun Liu[2], Yue Deng[1], Lei Wang[4], David C. Bock[4], Cherno Jaye[5], Duhan Zhang[6], Esther S. Takeuchi[3,4,7], Kenneth J. Takeuchi[3,4], Amy C. Marschilok[3,4,7], Lynden A. Archer[1,2]†

The propensity of metals to form irregular and nonplanar electrodeposits at liquid-solid interfaces has emerged as a fundamental barrier to high-energy, rechargeable batteries that use metal anodes. We report an epitaxial mechanism to regulate nucleation, growth, and reversibility of metal anodes. The crystallographic, surface texturing, and electrochemical criteria for reversible epitaxial electrodeposition of metals are defined and their effectiveness demonstrated by using zinc (Zn), a safe, low-cost, and energy-dense battery anode material. Graphene, with a low lattice mismatch for Zn, is shown to be effective in driving deposition of Zn with a locked crystallographic orientation relation. The resultant epitaxial Zn anodes achieve exceptional reversibility over thousands of cycles at moderate and high rates. Reversible electrochemical epitaxy of metals provides a general pathway toward energy-dense batteries with high reversibility.

E lectrodeposition is a two-century-old electrochemical method for creating thin, conformal coatings of metals on electrically conducting substrates. The method has in recent years reemerged as an area of scientific and technological interest owing to the role electrodeposition plays in the reversibility of energy storage in secondary/rechargeable batteries that use active metals—including lithium (Li), sodium (Na), potassium (K), magnesium (Mg), calcium (Ca), zinc (Zn), and aluminum (Al)—as anodes (1–4). The propensity of metals to form rough, nonuniform electrodeposits is a barrier to practical batteries because it leads to active material loss through multiple mechanisms (5–11). It is also dangerous because short circuits created when the nonuniform or dendritic metal electrodeposits proliferate in the interelectrode space to bridge the electrodes (Fig. 1A, left) can lead to fire or explosion.

In an epitaxial electrodeposition process, a thin-film electrodeposit forms a coherent or semicoherent lattice interface with the substrate. The single crystalline new phase (epilayer) exhibits a correlated orientation in relation to the substrate and low residual stresses. The strongest orientation correlations are achieved through directed nucleation and growth of the epilayer on a substrate that imposes minimal lattice strain. The process can be used to deposit metals, such as copper (Cu) (12, 13) and platinum (Pt) (14)—on substrates of different chemistries. Textured interphases that add negligibly to the mass of a battery electrode and form low-lattice-mismatch interfaces are of specific interest in the present study. Furthermore, because the epilayer and substrate can be composed of the same (homo-) or different (hetero-) materials, either homoepitaxy or heteroepitaxy could be used in the process.

During battery charging, an electrochemically inactive interphase with selected crystal symmetry and lattice parameters would ideally facilitate heteroepitaxial nucleation and growth of a metal anode in a strain-free state. Once the nucleates cover the substrate, the as-deposited metal layer would enable homoepitaxial deposition (Fig. 1A) to create uniform metal coatings. Upon discharging, the metal is stripped away, while the substrate remains intact and, therefore, available for a subsequent cycle of charge and discharge. Thus, the critical steps in implementing the concept are (i) identifying electrically conductive substrate materials that have crystallographic facets with low lattice mismatch with the metal anode of interest and (ii) fabrication of a macroscopic, textured substrate that preferentially exposes these facets.

We studied the morphology and reversibility of a zinc metal anode in a 2 mol/liter-ZnSO$_4$ aqueous electrolyte. This system is of interest because rechargeable batteries based on Zn anodes have remerged as an area of scientific and technological interest (15–17). The most important considerations in choosing Zn include (i) it has low reactivity and relatively low cost; (ii) the divalent Zn can be electrochemically coupled with low-cost cathode chemistries [for example, MnO$_2$ (18, 19)] in nonflammable aqueous electrolytes; and (iii) Zn anodes do not suffer from continuous parasitic reaction with electrolytes, which has plagued other metal anode batteries. The last of these attributes is the most important here because it allows us to focus on the atomic-scale processes that control the onset of morphological instability in the metal anode. Furthermore, Zn has a much higher Young's modulus (E) than that of alkali metals of contemporary interest as battery anodes ($E_{Zn} \approx 108$ GPa; $E_{Li} \approx 5$ GPa; $E_{Na} \approx 10$ GPa); once formed, Zn dendrites can more easily proliferate to cause

Fig. 1. Electrochemical growth pattern of Zn. (**A**) Scheme illustrating the design principle of epitaxial metal electrodeposition. (**B** and **C**) Scanning electron microscopy (SEM) images and (**D**) HAADF-STEM image of Zn electrodeposits on bare stainless steel from aqueous electrolyte current density $J = 4$ mA/cm^2.
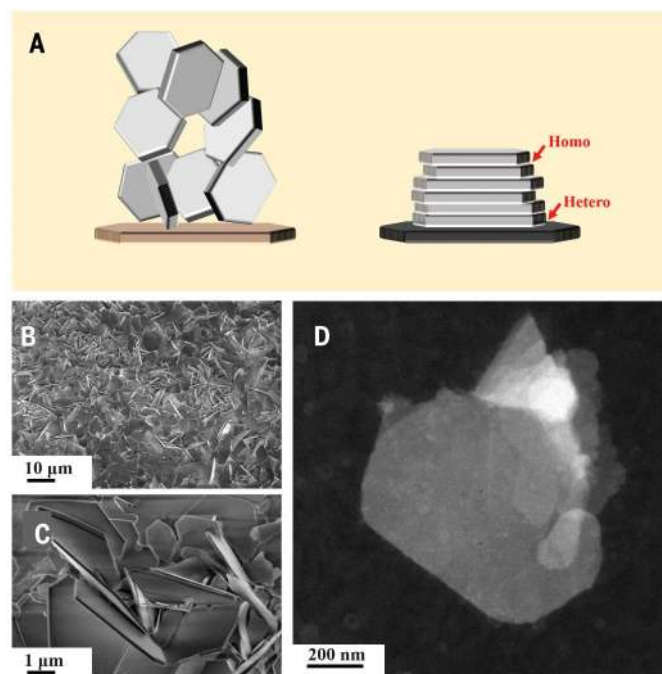
[1]Department of Materials Science and Engineering, Cornell University, Ithaca, NY 14853, USA. [2]Robert Frederick Smith School of Chemical and Biomolecular Engineering, Cornell University, Ithaca, NY 14853, USA. [3]Department of Chemistry, Stony Brook University, Stony Brook, NY 11794, USA. [4]Energy Sciences Directorate, Brookhaven National Laboratory, Interdisciplinary Sciences Building, Building 734, Upton, NY 11973, USA. [5]Material Measurement Laboratory, National Institute of Standards and Technology, Gaithersburg, MD 20899, USA. [6]Sibley School of Mechanical and Aerospace Engineering, Cornell University, Ithaca, NY 14853, USA. [7]Department of Materials Science and Chemical Engineering, Stony Brook University, Stony Brook, NY 11794, USA.
*These authors contributed equally to this work.
†Corresponding author. Email: laa25@cornell.edu

battery failure by metal orphaning (20) or short-circuiting (21) mechanisms.

The intrinsic growth mode of electrodeposited Zn is shown in Fig. 1, B to D. Zn exhibits a strong tendency to deposit as platelets, implying that a lower thermodynamic free energy is associated with the exposed closest packed plane—(0002) in hexagonal close-packed (hcp) metal (22). High-angle annular dark field scanning transmission electron microscopy (HAADF-STEM) (Fig. 1D, and fig. S1, energy-dispersive x-ray spectroscopy mapping) confirmed the plate-like morphology. The electron diffraction pattern (fig. S2) shows that the plane normal of the Zn plate is $[0001]_{Zn}$. Therefore, a candidate substrate for epitaxial electrodeposition of Zn should show similar atomic arrangement to the $(0002)_{Zn}$ plane (fig. S3).

A preliminary screening based on crystal structure was performed. Criteria included (i) does the crystal plane exhibit a small lattice misfit with $(0002)_{Zn}$. Numerically, the lattice misfit should be no larger than 25% as an empirical value to form a coherent or semi-coherent interface (23). (ii) Does the crystal plane of interest have a low lattice index? A low lattice index is preferred because it indicates higher atomic packing density and therefore higher surface stability (24). And

(iii) the substrate should remain intact and therefore electrochemically inactive during cycling. Within this screening framework, graphene stands out as a candidate material that meets all the specified criteria (fig. S3).

Creating a macroscopic material in which the basal plane of graphene is parallel to an electrode surface is not straightforward. We designed a fluid-based route for creating aligned graphene coatings. The method takes advantage of the ease with which high-aspect-ratio graphene flakes in a slurry are aligned by shear flow (25). The rheological properties of the graphene suspensions are shown in Fig. 2A. The initially elastic slurry ($G' > 10*G''$) yields at a low shear strain ($\gamma \approx 0.05$) and transitions to a liquid-like state at high strain in which $G'' > G'$. Correlations between graphene sheets are evidently broken in a modest shear flow. In continuous shear, the suspensions are shear-thinning at low rates $\dot{\gamma}(\sim 10^{-2}\,s^{-1})$ (fig. S4), and relaxation after cessation of shear is a two-step process (fig. S5), with the slower step lasting several hundreds of seconds. Subjecting a graphene suspension to a moderate shear rate for even a short period of time could therefore produce relatively long-lived orientation parallel to the shear plane.

We designed a doctor-blade–type apparatus to implement this process using suspensions composed of graphene flakes in N-methyl-2-pyrrolidone (NMP). To lock in the alignment, the sheared coatings were immediately transferred to a vacuum chamber, where the NMP solvent was removed. The effectiveness of the method can be seen by comparing morphologies and polarized near-edge x-ray absorption fine structure (NEXAFS) spectra of the graphene coating prepared with (Fig. 2B) and without (Fig. 2C) shearing (fig. S6 to S9). It is evident that our approach provides a simple, scalable route toward planar interphases composed of well-aligned graphene sheets with $[0001]_{graphene}$ facets perpendicular to the substrate.

In contrast to the deposition morphology on stainless steel (Fig. 1, B and C), in which Zn platelets are randomly oriented, Zn deposits formed on graphene are well directed, showing a locked orientation relation with the graphene substrate (Fig. 3 and fig. S10). Further analysis reveals that there are two stages in the epitaxial electrodeposition: stage I, heteroepitaxy between Zn and graphene (Fig. 3, A to D), and stage II, homoepitaxy of Zn after the graphene surface has been fully occupied (Fig. 3, E and F). Small newly deposited Zn layers are attached to the surface of the Zn formed in stage I (Fig. 3F and fig. S11). The Zn deposition rate on graphene appears lower than that on a bare stainless-steel substrate because the epitaxial regulation produces thin plates that are parallel to the substrate, more uniform, and compact, as schematically illustrated in Fig. 1A. This highly ordered growth is sustained at the high current density of 40 mA/cm² (fig. S12). Atomic force microscopy (fig. S13) and x-ray diffraction (figs. S14 to S16) results confirmed the epitaxial regulation of Zn deposition. As a comparison, no epitaxial growth was observed on Ketjen black–coated (an isotropic carbon) stainless steel (fig. S17). The plating and stripping of Zn was studied by means of cyclic voltammetry (CV) (fig. S18), and the results show no obvious impact of the deposition process on the electrochemical reaction mechanism.

When used as a battery anode, a successful metal electrode must be reversibly plated and stripped over hundreds or thousands of charge-discharge cycles. The coulombic efficiency (CE) is a measure of this reversibility. We quantified the CE for epitaxially and nonepitaxially deposited Zn using a procedure in which a certain amount of metal is plated on the substrate and then stripped away; the ratio of charge passed in each segment of the cycle determines the CE. Zn plating and stripping on an electrochemically inert substrate, such as stainless steel, shows CE values around 80% (fig. S19). These cells quickly fail, however, after only 20 plate-strip cycles. The observed voltage fluctuations are consistent with failure either as a result of
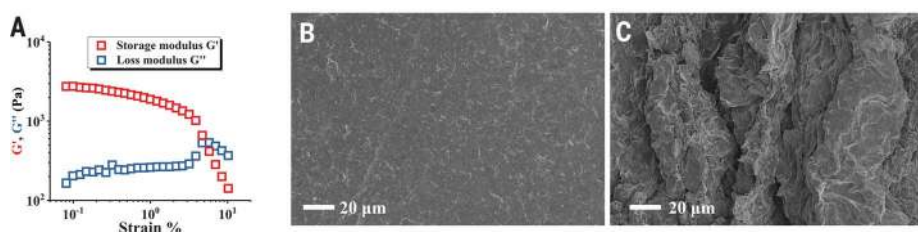

Fig. 2. Preparation of the epitaxial substrate in which graphene sheets are parallel to the substrate. (**A**) Strain sweep of the 4% graphene in NMP slurry. (**B** and **C**) SEM images of graphene membranes prepared (B) with and (C) without the shearing.
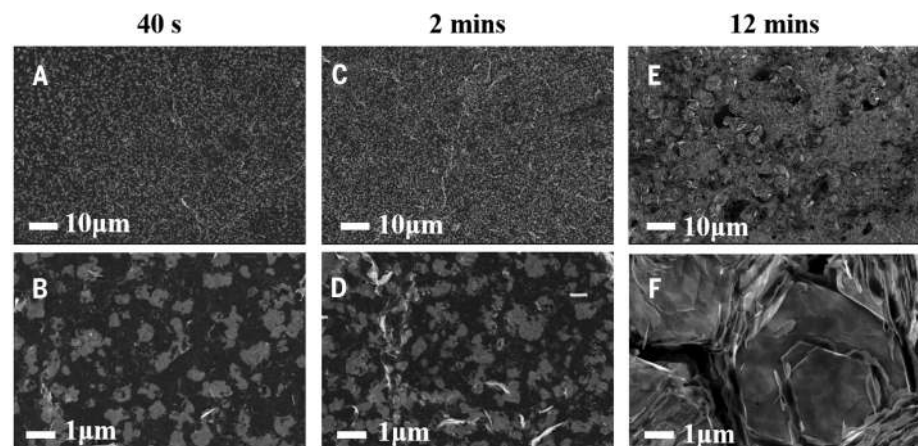

Fig. 3. SEM of Zn deposits on graphene-coated stainless steel. SEM deposition times, (**A** and **B**) 40 s, (**C** and **D**) 2 min, and (**E** and **F**) 12 min. Current density, J = 4 mA/cm².
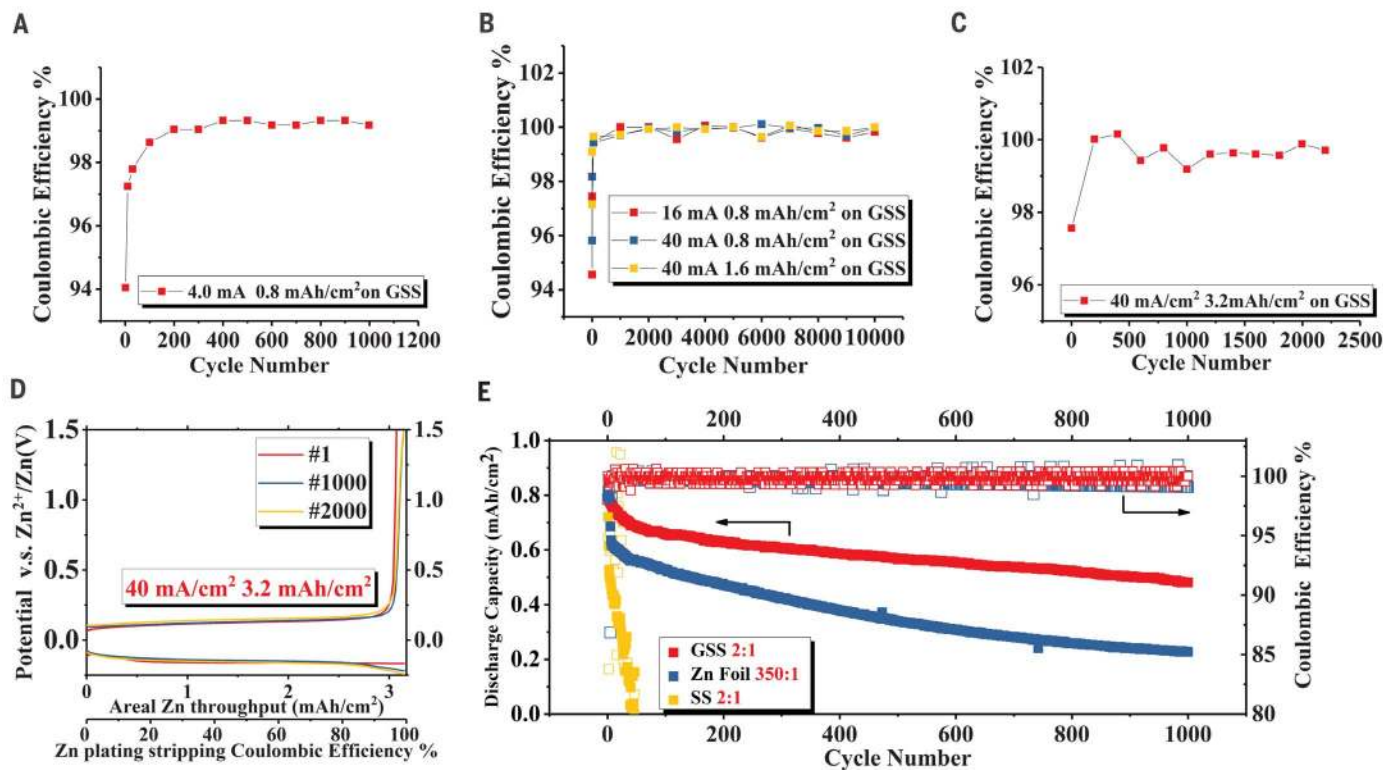
Fig. 4. Electrochemical performance of epitaxial Zn metal anodes. (**A**) CE at moderate current density on graphene coated stainless steel (GSS) substrate. (**B**) CE at high current densities on GSS. (**C**) CE under high current and high areal capacity condition on GSS. (**D**) The corresponding voltage profile. (**E**) Cycling performance of Zn||α-MnO₂ full cells with and without graphene, with controlled N:P electrode capacity ratios.

Table 1. Potential epitaxial substrates for anode metals.

Anode metal	Potential epitaxial substrate	Lattice misfit δ %
Al	Au/Ag	0.7/0.7
Ca	Sr/Pb	8/11
Zn	Co/Ti	6/9
Mg	Zr/Ti	0.9/8
Li	Ta	6
Na	Eu	8
K	Ba	4

localized short circuiting or by reconnection of fragmentary Zn deposits that broke away from the electrode ("orphaned" Zn) (figs. S20 and S21) (*21*). By contrast, epitaxial deposition of Zn yields quite noticeable improvements in reversibility (CE > 99% over 1000 cycles) (Fig. 4A).

We measured the CE at higher current densities of 16 and 40 mA/cm² (table S1) (*17, 26, 27*). As reported in Fig. 4B, high CE values (CE = 99.9% over 10,000 cycles) were observed. By contrast, electrodes without the graphene coating fail after just eight cycles (fig. S22). We also evaluated the performance of unaligned graphene substrates, created without the shearing procedure. With erratic voltage behavior, the measured average CE was 94%, and the cells failed by 125 cycles, which

is attributable to the uneven Zn deposition morphology (fig. S23).

We increased the areal Zn throughput to 3.2 mAh/cm² to assess the stability of the homoepitaxy component of the deposition. High electrode reversibility (CE ≈ 99.7% over 2000 cycles), stable voltage profiles, and homoepitaxial regulation of deposition morphology are reported in Fig. 4, C to D (fig. S24). By contrast, the unmodified electrode fails after the first cycle.

The high reversibility of the epitaxial anode allowed us to study rechargeable batteries with low negative-to-positive electrode capacity (N:P) ratio (*28, 29*). A low N:P ratio is required for high overall energy density of a battery (fig. S25). We created electrochemical

cells in which the epitaxial Zn anode is paired with a conventional α-MnO₂ cathode with a N:P ratio of 2:1. The cell with the epitaxial Zn anode maintains excellent capacity retention over 1000 cycles at 8 mA/cm² (Fig. 4E and fig. S26). Analogous Zn||MnO₂ cell cycling results at the same current density, but using anodes composed, respectively, of a Zn coating on stainless steel (N:P = 2:1) and a 620-μm-thick Zn foil (N:P ~ 350:1) are provided in Fig. 4E.

In addition to aqueous electrolytes, the results in fig. S27 to S29 reveal that the epitaxial approach can be readily extended to other electrolytes of interest, such as 0.2 mol/liter Zn (CF₃SO₃)₂ in dimethylether. In this nonaqueous electrolyte, a 99.97% CE was achieved. The improvement could stem from the suppression of hydrogen evolution and other side reactions.

Epitaxial electrodeposition as a strategy for creating highly reversible metal anodes is relevant for other electrode chemistries of contemporary interest. For face-centered cubic (FCC) metals (Al and Ca), body-centered cubic (BCC) metals (Li, Na, and K), and HCP metals (Mg), the screening for potential substrates can be performed on the basis of the atomic arrangements of their closely packed planes. Previously, epitaxial electrodeposition of various metals has been demonstrated (*30, 31*). Although none of these efforts have considered

reversibility of the process, they indicate that the concept is broadly useful. In line with the criteria used to screen epitaxial substrates for Zn, we performed a screening for potential substrates for FCC, HCP, and BCC metals (Table 1 and tables S2 to S4). As a demonstration, we studied the morphology of Al on (111)–textured gold (Au) nanosheets (32). This pairing stands out for the small lattice misfit $\delta_{Au-Al} = 0.7\%$ and chemical inertness of Au. We also performed electrodeposition in a Lewis-acidic electrolyte that can dissolve surface oxide layer (33, 34), which may prevent direct contact between the metals and the substrate. The results reported in figs. S30 and S31 show that the Au sheets facilitate formation of evenly distributed, nanosized Al electrodeposits, in contrast to the uneven, coarse particulate Al morphologies formed in the absence of epitaxial regulation.

We report that reversible epitaxial electrodeposition at a metal electrode can be achieved by using textured electrically conducting electrode coatings with low lattice mismatch with the metal of interest. An epitaxial aqueous-Zn anode is reported to achieve high reversibility (CE > 99.7%) at moderate and high current densities. The epitaxy regulation concept can be extended to achieve reversible cycling in nonaqueous-Zn electrochemical cells as well as in other rechargeable batteries that use metals as anode.

REFERENCES AND NOTES

1. J. F. Parker et al., Science 356, 415–418 (2017).
2. D. Lin, Y. Liu, Y. Cui, Nat. Nanotechnol. 12, 194–206 (2017).
3. M. S. Whittingham, Science 192, 1126–1127 (1976).
4. M.-C. Lin et al., Nature 520, 325–328 (2015).
5. M. D. Tikekar, S. Choudhury, Z. Tu, L. A. Archer, Nat. Energy 1, 16114 (2016).
6. Y. Li et al., Science 358, 506–510 (2017).
7. M. J. Zachman, Z. Tu, S. Choudhury, L. A. Archer, L. F. Kourkoutis, Nature 560, 345–349 (2018).
8. P. Bai, J. Li, F. R. Brushett, M. Z. Bazant, Energy Environ. Sci. 9, 3221–3229 (2016).
9. K. E. K. Sun et al., ACS Appl. Mater. Interfaces 9, 9681–9687 (2017).
10. A. Pei, G. Zheng, F. Shi, Y. Li, Y. Cui, Nano Lett. 17, 1132–1139 (2017).
11. R. F. Voss, M. Tomkiewicz, J. Electrochem. Soc. 132, 371–375 (1985).
12. C. M. Hull, J. A. Switzer, ACS Appl. Mater. Interfaces 10, 38596–38602 (2018).
13. S. Hwang, I. Oh, J. Kwak, J. Am. Chem. Soc. 123, 7176–7177 (2001).
14. K. Uosaki et al., J. Phys. Chem. B 101, 7566–7572 (1997).
15. A. R. Mainar et al., J. Energ. Stor. 15, 304–328 (2018).
16. D. Kundu, B. D. Adams, V. Duffort, S. H. Vajargah, L. F. Nazar, Nat. Energy 1, 16119 (2016).
17. F. Wang et al., Nat. Mater. 17, 543–549 (2018).
18. N. Zhang et al., Nat. Commun. 8, 405 (2017).
19. G. G. Yadav et al., Nat. Commun. 8, 14424 (2017).
20. J. Zheng et al., ACS Energy Lett. 4, 1349–1355 (2019).
21. S. Higashi, S. W. Lee, J. S. Lee, K. Takechi, Y. Cui, Nat. Commun. 7, 11801 (2016).
22. R. Sato, J. Electrochem. Soc. 106, 206–211 (1959).
23. D. A. Porter, K. E. Easterling, M. Sherif, Phase Transformations in Metals and Alloys (Revised Reprint) (CRC, 2009).
24. C. Klein, B. Dutrow, J. D. Dana, Manual of Mineral Science (Wiley, ed. 23, 2007).
25. G. Natale, N. K. Reddy, R. K. Prud'homme, J. Vermant, Phys. Rev. Fluids 3, 063303 (2018).
26. A. Naveed, H. Yang, J. Yang, Y. Nuli, J. Wang, Angew. Chem. 131, 2786–2790 (2019).
27. S.-D. Han et al., ACS Appl. Mater. Interfaces 8, 3021–3031 (2016).
28. P. Albertus, S. Babinec, S. Litzelman, A. Newman, Nat. Energy 3, 16–21 (2018).
29. J. Zheng et al., ACS Energy Lett. 4, 271–275 (2018).
30. J. Petermann, G. Broza, J. Mater. Sci. 22, 1108–1112 (1987).
31. P. Allongue, F. Maroun, Curr. Opin. Solid State Mater. Sci. 10, 173–181 (2006).
32. C. C. Li et al., Adv. Funct. Mater. 16, 83–90 (2006).
33. Q. Zhao et al., Sci. Adv. 4, eaau8131 (2018).
34. N. Jayaprakash, S. K. Das, L. A. Archer, Chem. Commun. 47, 12610–12612 (2011).

Science

Reversible epitaxial electrodeposition of metals in battery anodes

Jingxu Zheng, Qing Zhao, Tian Tang, Jiefu Yin, Calvin D. Quilty, Genesis D. Renderos, Xiaotun Liu, Yue Deng, Lei Wang, David C. Bock, Cherno Jaye, Duhan Zhang, Esther S. Takeuchi, Kenneth J. Takeuchi, Amy C. Marschilok and Lynden A. Archer

Controlling electrode growth

Batteries with metal anodes can grow dendrites during cycling, which can cause short circuits in a battery or subsequently reduce the charge capacity. Zheng *et al.* developed a process to electrodeposit zinc on a graphene-coated stainless-steel electrode, such that the zinc forms plates with preferential orientation parallel to the electrode. This is achieved by depositing a graphene layer on stainless steel designed to epitaxially match the basal (002) plane of metallic zinc, minimizing lattice strain. During cycling, the zinc will redeposit in plate form rather than as a dendrite such that the batteries show excellent reversibility over thousands of cycles.

Science, this issue p. 645

ARTICLE TOOLS	http://science.sciencemag.org/content/366/6465/645
SUPPLEMENTARY MATERIALS	http://science.sciencemag.org/content/suppl/2019/10/30/366.6465.645.DC1
REFERENCES	This article cites 36 articles, 6 of which you can access for free http://science.sciencemag.org/content/366/6465/645#BIBL
PERMISSIONS	http://www.sciencemag.org/help/reprints-and-permissions